Supporting information

Self-assembly of Porphyrin Nanostructures at the Interface between Two Immiscible Liquids

Andrés F. Molina-Osorio,[1] David Cheung,[2] Colm O'Dwyer,[3,4] Andrew A. Stewart,[5] Manuel Dossot,[6] Grégoire Herzog,[6] and Micheál D. Scanlon.[1,*]

[1]The Bernal Institute and Department of Chemical Sciences, School of Natural Sciences, University of Limerick (UL), Limerick V94 T9PX, Ireland.

[2]School of Chemistry, National University of Ireland, Galway, University Road, Galway, Ireland.

[3]School of Chemistry, and Tyndall National Institute, University College Cork, Cork, T12 YN60 Ireland.

[4]Advanced Materials and Bioengineering Research (AMBER) centre.

[5]The Bernal Institute and Department of Physics, School of Natural Sciences, University of Limerick (UL), Limerick V94 T9PX, Ireland.

[6]CNRS-Université de Lorraine, LCPME UMR 7564, 405 Rue de Vandoeuvre, 54600 Villers-lès-Nancy, France.

Supporting Experimental Methods

***In situ* microscopy.** The films of Por-INs were very well adhered to the aqueous-TFT interface (see Figure 1a and Figure S1). This attribute significantly facilitated their subsequent unambiguous *in situ* spectroscopic characterisation as it allowed the selective removal of the bulk porphyrin molecules from solution. The absorption or emission of light by the latter would otherwise greatly interfere with the selective *in situ* acquisition of UV/vis absorption or fluorescence emission spectra from the Por-INs.

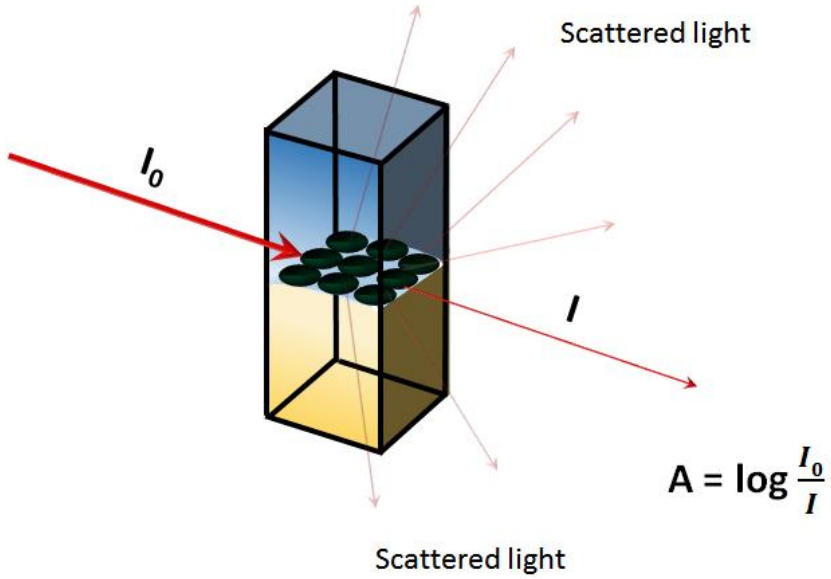

Figure S1. Schematic of the experimental configuration implemented to obtain *in situ* UV/vis absorbance and steady-state fluorescence spectra of the Por-INs.

Molecular dynamic simulations. Simulations of interfacial adsorption and assembly were performed using a pre-equilibrated water | TFT interface, consisting water and TFT regions with 4000 water molecules and 1226 TFT molecules, respectively. For the dimerisation free energy calculations two porphyrin molecules were placed in a box containing 4000 water molecules. The porphyrin and TFT molecules were modelled using the Generalised Amber Force Field[1] and the TIP3P model was used for the water molecules. Charges on the zinc porphyrin unit were found using the Metal Center Parameter Builder.[2] Charges on the sidechains and TFT were determined from AM1-BCC calculations.[3,4] Bonded potentials for the Zn atom were taken from the work of Lin and Wang.[5] Force field setup and parameterisation were performed using the Antechamber program in AmberTools (version 14). Full details of the force field, along with sample input files are detailed *vide infra*.

All simulations were performed using the LAMMPS molecular dynamics package.[6] The simulation temperature and pressure were 298 K and 1 atm, with temperature and pressure controlled using Nose-Hoover thermostat (relaxation time 0.2 ps) and barostats (relaxation 2 ps).[6] For interfacial simulations the box was allowed to vary in the *x* and *y* dimensions (the z box length was held fixed). Electrostatic interactions were evaluated using a particle-particle-particle-mesh sum.[7] For interface simulations convergence parameter $\alpha = 0.263$ A^{-1} and a reciprocal space grid of 36 x 36 x 80 was used, for simulations in bulk water $\alpha = 0.278$ A^{-1} and a reciprocal space grid of 40 x 40 x 40 was used. Van der Waals interactions were cut-off at 11 A, with tail corrections applied to both energy and force. Adsorption and dimerization free energies were found using the Adaptive Biasing Force (ABF) method.[8,9] To assist convergence the full z and r range were divided into 5 A wide windows, with ABF used to generate the free energy profile in each window.

Force field details

Atom types. The atom names for the porphyrin are shown below (two rings are given explicitly, atom names for the other rings can be found by equivalence). For the free base the nitrogen atoms NA and NC are bonded to hydrogens (HA and HC)

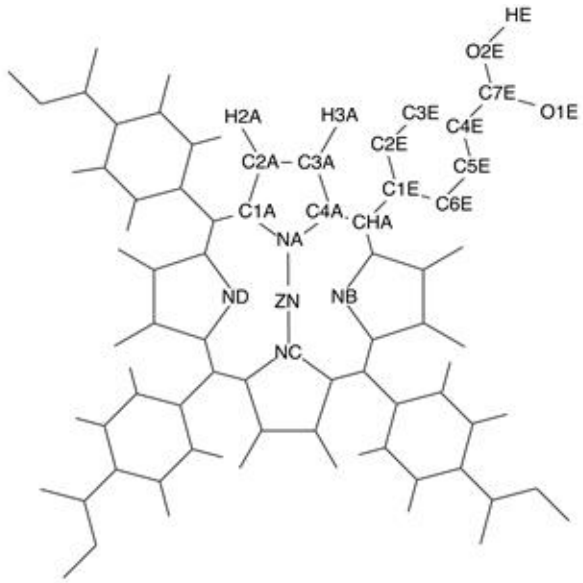

Non-bonded parameters

$[ZnTPPc]^{4-}$

Atom	Atom type	q / e	ε / kcal mol^{-1}	σ / A
C1A, C1B, C1C, C1D, C4A, C4B, C4C,C4D	ca	+0.498	0.086	3.40
C2A, C2B, C2C, C2D, C3A, C3B, C3C, C3D	ca	-0.275	0.086	3.40
H2A, H2B, H2C, H2D, H3A, H3B, H3C, H3D	ha	+0.165	0.015	2.60
NA, NC	nc	-0.710	0.170	3.25
NB, ND	nd	-0.710	0.170	3.25
CHA, CHB, CHC, CHD	cg	-0.249	0.086	3.40
ZN	ZN	+1.132	0.0125	1.96
C1E, C1F, C1G, C1H	ca	-0.162	0.086	3.40
C2E, C2F, C2G, C2H, C6E, C6F, C6G, C6H	ca	-0.166	0.086	3.40
H2E, H2F, H2G, H2H, H6E, H6F, H6G, H6H	ha	+0.101	0.015	2.60
C3E, C3F, C3G, C3H, C5E, C5F, C5G, C5H	ca	-0.109	0.086	3.40
H3E, H3F, H3G, H3H, H5E, H5F, H5G, H5H	ha	+0.148	0.015	2.60
C4E, C4F, C4G, C4H	ca	-0.124	0.086	3.40
C7E, C7F, C7G, C7H	c	+0.906	0.086	3.40
O1E, O1F, O1G, O1H, O2E, O2F, O2G, O2H	o	-0.834	0.210	2.96

H_4[ZnTPPc]

Atom	Atom type	q / e	ε / kcal mol^{-1}	σ / A
C1A, C1B, C1C, C1D, C4A, C4B, C4C,C4D	ca	+0.498	0.086	3.40
C2A, C2B, C2C, C2D, C3A, C3B, C3C, C3D	ca	-0.275	0.086	3.40
H2A, H2B, H2C, H2D, H3A, H3B, H3C, H3D	ha	+0.165	0.015	2.60
NA, NC	nc	-0.710	0.170	3.25
NB, ND	nd	-0.710	0.170	3.25
CHA, CHB, CHC, CHD	cg	-0.518	0.086	3.40
ZN	ZN	+1.132	0.0125	1.96
C1E, C1F, C1G, C1H	ca	-0.094	0.086	3.40
C2E, C2F, C2G, C2H, C6E, C6F, C6G, C6H	ca	-0.148	0.086	3.40
H2E, H2F, H2G, H2H, H6E, H6F, H6G, H6H	ha	+0.141	0.015	2.60
C3E, C3F, C3G, C3H, C5E, C5F, C5G, C5H	ca	-0.069	0.086	3.40
H3E, H3F, H3G, H3H, H5E, H5F, H5G, H5H	ha	+0.157	0.015	2.60
C4E, C4F, C4G, C4H	ca	-0.138	0.086	3.40
C7E, C7F, C7G, C7H	c	+0.652	0.086	3.40
O1E, O1F, O1G, O1H	o	-0.554	0.210	2.96
O2E, O2F, O2G, O2H	oh	-0.608	0.210	2.96
HE, HF, HG, HH	ho	+0.447	0	0

$[H_2TPPc]^{4-}$

Atom	Atom type	q / e	ε / kcal mol^{-1}	σ / A
C1A, C1B, C1C, C1D, C4A, C4B, C4C,C4D	ca	+0.0417	0.086	3.40
C2A, C2B, C2C, C2D, C3A, C3B, C3C, C3D	ca	-0.0364	0.086	3.40
H2A, H2B, H2C, H2D, H3A, H3B, H3C, H3D	ha	+0.0639	0.015	2.60
NA, NC	nc	-0.355	0.170	3.25
HA, HC	hn	+0.166	0.016	1.069
NB, ND	nd	-0.247	0.170	3.25
CHA, CHB, CHC, CHD	cg	+0.151	0.086	3.40
C1E, C1F, C1G, C1H	ca	-0.162	0.086	3.40
C2E, C2F, C2G, C2H, C6E, C6F, C6G, C6H	ca	-0.166	0.086	3.40
H2E, H2F, H2G, H2H, H6E, H6F, H6G, H6H	ha	+0.101	0.015	2.60
C3E, C3F, C3G, C3H, C5E, C5F, C5G, C5H	ca	-0.109	0.086	3.40
H3E, H3F, H3G, H3H, H5E, H5F, H5G, H5H	ha	+0.148	0.015	2.60
C4E, C4F, C4G, C4H	ca	-0.124	0.086	3.40
C7E, C7F, C7G, C7H	c	+0.906	0.086	3.40
O1E, O1F, O1G, O1H, O2E, O2F, O2G, O2H	o	-0.834	0.210	2.96

$H_4[H_2TPPc]$

Atom	Atom type	q / e	ε / kcal mol^{-1}	σ / A
C1A, C1B, C1C, C1D, C4A, C4B, C4C,C4D	ca	+0.0417	0.086	3.40
C2A, C2B, C2C, C2D, C3A, C3B, C3C, C3D	ca	-0.0364	0.086	3.40
H2A, H2B, H2C, H2D, H3A, H3B, H3C, H3D	ha	+0.0639	0.015	2.60
NA, NC	nc	-0.355	0.170	3.25
HA, HC	hn	+0.166	0.016	1.069
NB, ND	nd	-0.247	0.170	3.25
CHA, CHB, CHC, CHD	cg	+0.151	0.086	3.40
C1E, C1F, C1G, C1H	ca	-0.094	0.086	3.40
C2E, C2F, C2G, C2H, C6E, C6F, C6G, C6H	ca	-0.148	0.086	3.40
H2E, H2F, H2G, H2H, H6E, H6F, H6G, H6H	ha	+0.141	0.015	2.60
C3E, C3F, C3G, C3H, C5E, C5F, C5G, C5H	ca	-0.069	0.086	3.40
H3E, H3F, H3G, H3H, H5E, H5F, H5G, H5H	ha	+0.157	0.015	2.60
C4E, C4F, C4G, C4H	ca	-0.138	0.086	3.40
C7E, C7F, C7G, C7H	c	+0.652	0.086	3.40
O1E, O1F, O1G, O1H	o	-0.554	0.210	2.96
O2E, O2F, O2G, O2H	oh	-0.608	0.210	2.96
HE, HF, HG, HH	ho	+0.447	0	0

Trifluorotoluene

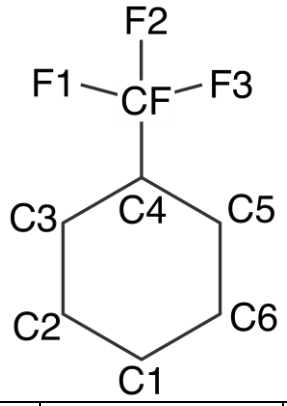

Atom	Atom type	q / e	ε / kcal mol^{-1}	σ / A
C1	ca	-0.100	0.086	3.40
H1	ha	+0.139	0.015	2.60
C2, C6	ca	-0.134	0.086	3.40
H2, H6	ha	+0.142	0.015	2.60
C3, C5	ca	-0.081	0.086	3.40
H3, H5	ha	+0.151	0.015	2.60
C4	ca	-0.168	0.086	3.40
CF	c3	+0.687	0.109	3.40
F1, F2, F3	f	-0.238	0.061	3.118

Bonded parameters

Bond stretching and bond angle bending parameters for ZN atoms listed below. Other force field parameters are taken from the Generalized Amber Force Field.

Bond	k / kcal mol^{-1} A^{-2}	r_0 / A
ZN-nc	56	2.07
ZN-nd	56	2.07

Angle	k / kcal mol^{-2} rad^{-2}	θ_0 / degrees
nc-ZN-nc	31.1	180.0
nc-ZN-nd	31.1	90.0
nd-ZN-nd	31.1	180.0
ca-nc-ZN	47.65	126.5
ca-nd-ZN	47.65	126.5

Sample input files are available on request from the authors. For each simulated system (water-TFT interface with 1, 16, and 32 porphyrin molecules, each porphyrin dimer in water) a lammps input script and data file is included, along with parameter file containing GAFF parameters.

Cyclic voltammetry and photocurrent transient measurements. Cyclic voltammograms and photocurrent measurements using a DC illumination were performed in a specialised 4-electrode electrochemical cell, using the light emitting diode (LED) driver provided by Metrohm Autolab in conjunction with a PGSTAT204 in the configuration presented in Figure S2. The reference electrodes used were Ag/AgCl for the organic reference solution and Ag/AgCitrate for the aqueous electrolyte. The counter electrodes in each phase were Pt. The supporting electrolyte in the organic phase was bis(triphenylphosphoranylidene)ammonium tetrakis(pentafluorophenyl)borate (BATB). The light source was a trifocal LED with a beam width of 18° and $\lambda_{max.}$ of 470 nm. The emission spectrum of the LED, as well as the absorption spectra of ZnTPPc, H_2TPPc and their respective Por-INs are presented in Figure S3. As clearly illustrated in Figure S3, a major advantage of porphyrin nanostructure formation is the broadening of the absorption spectrum, a highly desirable trait when designing nanomaterials for use in solar energy conversion.[10] The broadening of the absorption spectra for ZnPor-INs and H_2Por-INs leads to a far greater overlap with the emission spectrum of the 470 nm LED in comparison to the aqueous solutions of ZnTPPc and H_2TPPc.

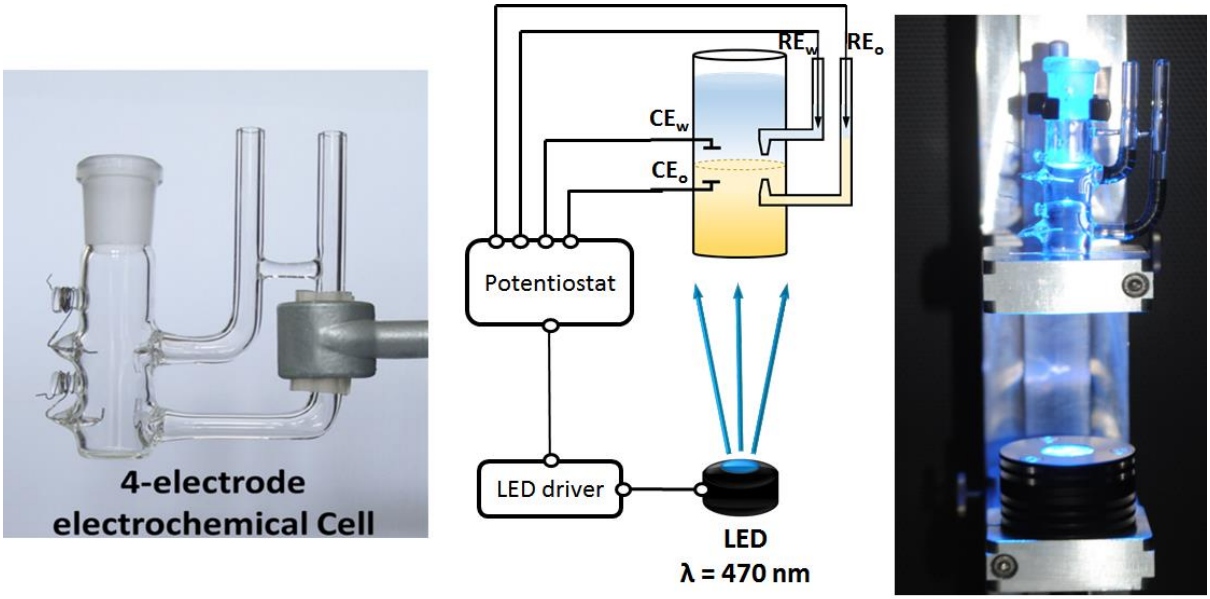

Figure S2. Image of the 4-electrode electrochemical cell, with a schematic and image of the setup used for photocurrent transient measurements. (CE_w and CE_o are the counter electrodes in the water and TFT phases, respectively, and RE_w and RE_o are the reference electrodes in each phase).

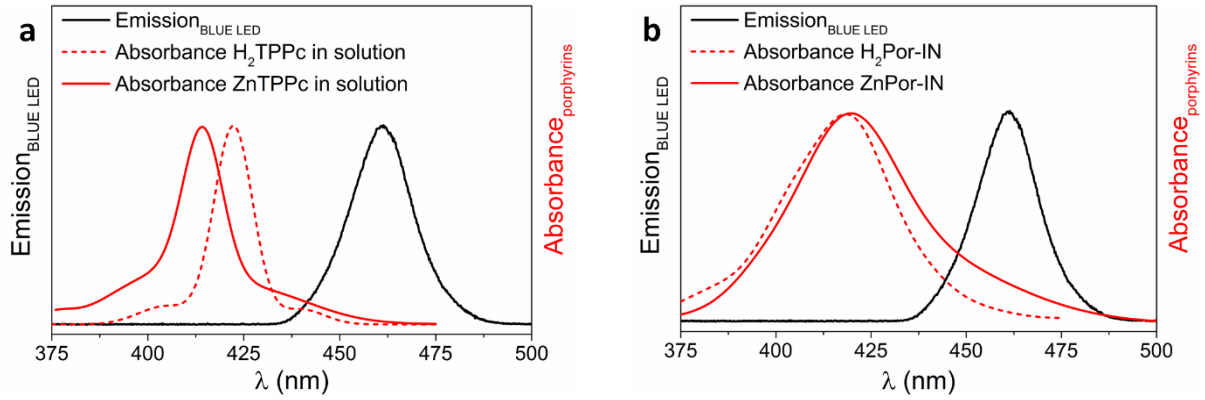

Figure S3. Overlaps between the emission of the blue LED and absorption of **a)** ZnTPPc and H_2TPPc in solution and **b)** their respective Por-INs.

The light intensity of the LED was controlled through the LED driver presented in Figure S4. This driver is a current source that converts an input voltage difference signal provided by the potentiostat to a current output signal directed to the LED. This conversion is performed using the Digital to Analog converter (DAC164) according to:

$$i_{\mathrm{LED}} = \left(\frac{i_{\mathrm{range}}}{\mathrm{V_{range}}}\right)\mathrm{V_{DAC164}} = \left(\frac{1000\ \mathrm{mA}}{10\ \mathrm{V}}\right)\mathrm{V_{DAC164}} = (100\ \mathrm{mA{\cdot}V^{-1}}){\cdot}\mathrm{V_{DAC164}}$$

where i_{LED} is the output driving current. For calculations, in order to convert this current to light intensity ($\mathrm{mW{\cdot}cm^{-2}}$) and photon flux ($\#\ \mathrm{photons{\cdot}s^{-1}{\cdot}cm^{-2}}$), the LED intensity was calibrated using a photodiode located at a controlled distance from the light source. The calibration was performed knowing the responsivity (R) of the photodiode and the area of the electrified liquid-liquid interface using the following relationship:

$$P\ (\mathrm{mW{\cdot}cm^{-2}}) = \frac{j_{\mathrm{photodiode}}\ (\mathrm{mA})}{\mathrm{Area}\ (\mathrm{cm^2}){\cdot}\mathrm{R}\ (\mathrm{mA{\cdot}mW^{-1}})}$$

The photon flux at each driving current was calculated from the light intensity knowing that the energy of a photon with a wavelength of 470 nm is 4.226×10^{-19} J. The results of these calculations are presented in Figure S4.

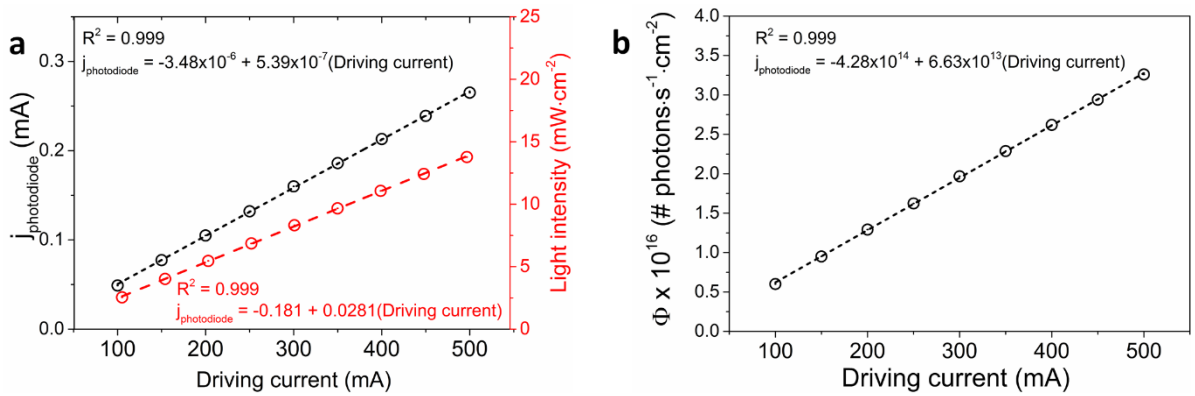

Figure S4. a) Photocurrents measured from the calibration photodiode at each driving current applied to the LED driver, and the calculated light intensity provided by the blue LED. **b)** The calculated photon flux at the electrified liquid-liquid interface at each driving current applied to the LED driver.

Supporting Figures and Tables

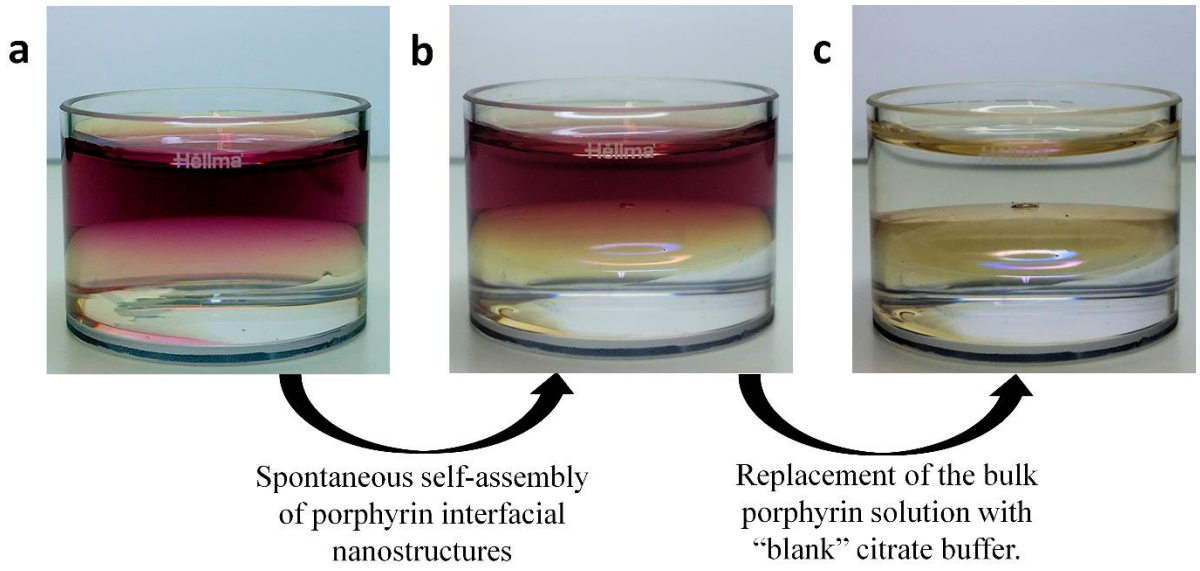

Figure S5. Methodology of porphyrin interfacial nanostructure formation. **a)** Aqueous solutions of ZnTPPc or H_2TPPc were typically prepared with 50 μM porphyrin present. Critically, the pH of the aqueous solution was adjusted using a 10 mM ionic strength lithium citrate buffer to match the p*K*a of the 4-carboxyphenyl substituents (pK_a^{COOH} = 5.8). Subsequently, aqueous solutions at pH 5.8 were contacted with α,α,α-trifluorotoluene (TFT), leading to a well-defined aqueous | organic interface. Note the top phase is the aqueous phase. **b)** Upon contact, the clear formation of porphyrin interfacial nanostructures (Por-INs) was immediately seen visually as a yellow/green complexion (image taken after one hour of contact). **c)** To isolate the Por-INs at the interface, the upper 50% of the volume of the aqueous phase was carefully removed by a pipette and replaced with porphyrin-free lithium citrate buffer. This procedure was repeated until no porphyrin was detectable in the aqueous phase by UV/vis spectroscopy. The Por-IN film remained intact and stable, with no re-dissolution observed after 1 day.

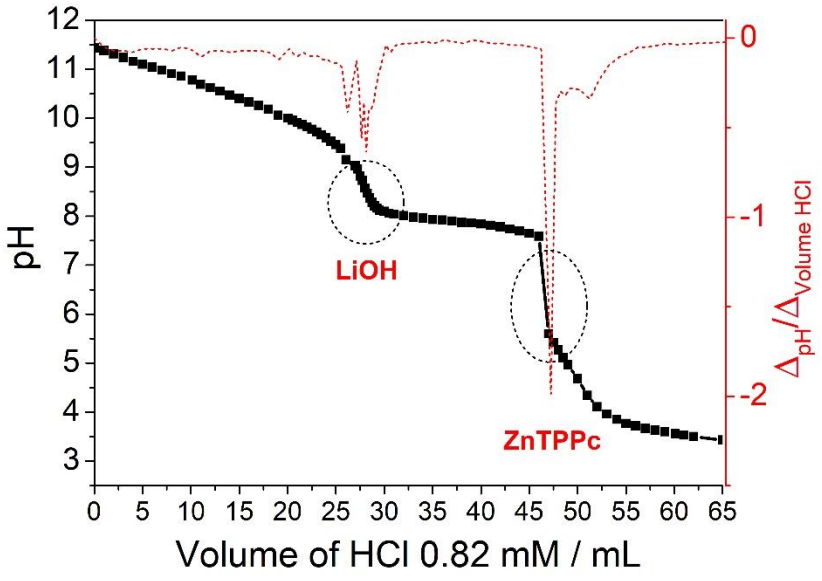

Figure S6. Determining the p*K*a of ZnTPPc by potentiometric titration. Potentiometric titration of a mixture of ZnTPPc 9.83 x 10^{-5} M and 3.90 x 10^{-2} M LiOH with 8.28 x 10^{-4} M HCl. The first equivalence point at 37.6 mL corresponds to the neutralization of LiOH and the second to the neutralisation of ZnTPPc.

Discussion | Only one p*K*a was observed for the potentiometric titration of ZnTPPc with HCl. This suggests that the different p*K*a values of the carboxylic groups fall within a very narrow interval of pH and that for clarity purposes, a global p*K*a can be a good approximation.

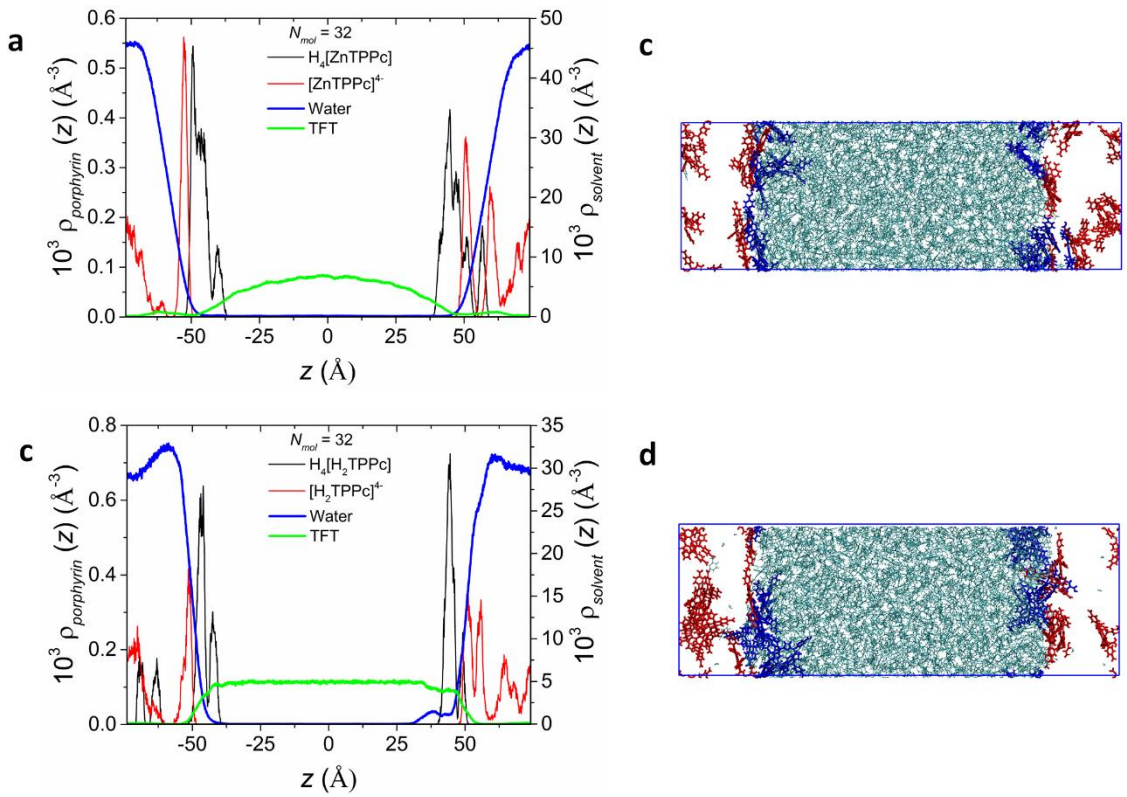

Figure S7. Molecular dynamic studies demonstrating the layer-by-layer formation of the porphyrin interfacial nanostructures at the water | TFT interface. a) Density (ρ) profiles mimicking the situation at pH 5.8 (= pKa^{COOH}), averaged over 10 ns of molecular dynamics. The simulation consists of 16 fully deprotonated $[ZnTPPc]^{4-}$ molecules (red lines) and 16 fully protonated H_4[ZnTPPc] molecules (black lines). The density profiles of water (blue line) and TFT (green line) are also shown. b) A simulation snapshot of the water | TFT | water density profile with 16 $[ZnTPPc]^{4-}$ (red) and 16 H_4[ZnTPPc] (blue) molecules present in the aqueous phase. c) The density profile and d) simulation snapshot of the water | TFT | water density profiles for H_2TPPc adsorption, averaged over 10 ns of molecular dynamics.

Discussion | Free energy profiles (PMF) for the porphyrins at the water | TFT interface (Figure 1c) demonstrate that the charged $[ZnTPPc]^{4-}$ or $[H_2TPPc]^{4-}$ species, being more hydrophilic, have

a free energy minimum approximately 4 to 5 Å from the interface itself, while the neutral $H_4[H_2TPPc]$ or $H_4[ZnTPPc]$ molecules lie closer to the interface or on the TFT side of the interface. From the free energy profiles it can be seen that the porphyrins are only weakly bound to the interface, with desorption (into the aqueous layer) free energies of ~24 $kJ \cdot mol^{-1}$ and ~48 $kJ \cdot mol^{-1}$ for the charged and neutral species, respectively. A significantly higher barrier exists (>200 $kJ \cdot mol^{-1}$) for the penetration of these molecules into the TFT layer, indicative of their highly hydrophilic nature. Meanwhile, the neutral porphyrins are both somewhat hydrophobic, with a lower barrier to enter the TFT layer. For $H_4[H_2TPPc]$ the desorption free energy (into the TFT layer) is similar to that for the charged porphyrins (into the aqueous phase). This difference in the location of charged and neutral molecules affects the assembly of porphyrin molecules at the interface (Figure S7). Due to their more hydrophobic nature, the neutral porphyrins reside on the aqueous-TFT interface, forming an interfacial layer. The charged porphyrins partially adsorb onto this, with the neutral molecules acting as a template for the formation of the multilayer porphyrin interfacial nanostructures (Por-INs).

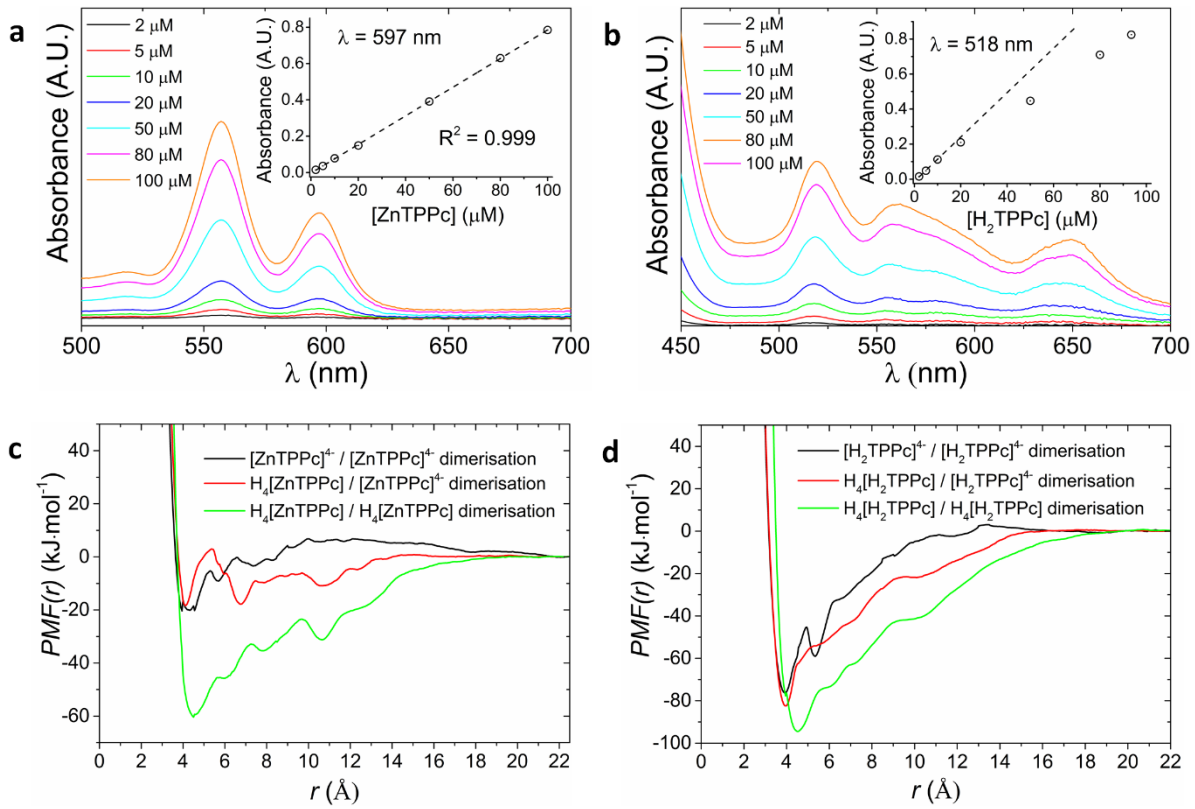

Figure S8. Investigating the tendency of ZnTPPc and H_2TPPc molecules in the bulk aqueous solution to dimerise or aggregate as a function of porphyrin concentration. UV/vis absorption spectra of aqueous solutions of increasing concentrations of a) ZnTPPc (2 to 100 μM) and b) H_2TPPc (2 to 100 μM) in lithium citrate buffer (10 mM ionic strength, pH 5.8). Insets: The increase in absorbance as a function of porphyrin concentration. Dimerisation free energies were determined using potential of mean force (PMF) calculations. PMF calculations were performed between both deprotonated and protonated c) ZnTPPc and d) H_2TPPc molecules to mimic (i) highly alkaline pH conditions with predominantly the anionic $[ZnTPPc]^{4-}$ or $[H_2TPPc]^{4-}$ species present, (ii) pKa^{COOH} conditions with 1:1 ratios of $[ZnTPPc]^{4-}$ - H_4[ZnTPPc] or $[H_2TPPc]^{4-}$ - $H_4[H_2TPPc]$ species in solution, and (iii) pH conditions with predominately H_4[ZnTPPc] or $H_4[H_2TPPc]$ molecules present in the range of 1 > pH < 5.

Discussion | For ZnTPPc, no deviation from the Beer-Lambert Law was observed as determined from the linear dependence of the absorbance of the Q band at 597 nm with increasing ZnTPPc concentration in solution (Figure S8a). Although a linear range of 2 – 100 μM is shown in Figure S8a, this was seen to extend as far as 500 μM (data not shown). Previous studies by Pasternack *et al.* have also concluded that ZnTPPc remains in a non-aggregated monomeric form at pH 6.8, *i.e.,* at pH values more alkaline than pKa^{COOH}, even in an aqueous solution with 10-times the ionic strength investigated herein.[11] This ability to resist dimerisation, or more extensive aggregation, in aqueous solutions is attributed to the penta-coordination of the zinc atom in ZnTPPc, with a water molecule occupying the axial position.[12–15] The axial water ligand prevents close approach of porphyrin molecules. More subtly, axial coordination of metalloporphyrins leads to the metal ion being displaced from the porphyrin ring plane.[16] The latter may have a disruptive effect on the π-electron density distribution within the core of the macrocycle, weakening the Van der Waals interactions responsible for dimer or higher aggregate formation with other porphyrin monomers.

In comparison, free-base porphyrins, such as H_2TPPc,[17,18] and metalloporphyrins with a coordination number of four, such as CuTPPc, that lack hydration in the axial position[11,13,19] dimerises and aggregate rapidly in aqueous solutions at pH values more alkaline than pKa^{COOH} in the presence of added electrolyte. Even modest amounts of added electrolyte will reduce the coulombic barrier to the close approach of other ionic species, such as another anionic H_2TPPc molecule, thereby leading to dimerisation and aggregation at a certain concentration of H_2TPPc in solution. The latter has been reported as >10 μM in 10 mM ionic strength buffer or > 1 μM with 100 mM of added electrolyte.[18] In broad agreement with these previous findings, we see a deviation from linearity of the absorbance of the Q band at 518 nm with increasing H_2TPPc concentration in solution (Figure S8b). The latter is indicative of H_2TPPc dimer formation for

concentrations >10 μM in 10 mM ionic strength lithium citrate buffer at pH 5.8. However, under these conditions no higher aggregates of H_2TPPc are formed, *i.e.* no spectral broadening or blue or red-shifting of the Soret or Q bands was observed, and no H_2TPPc aggregates were visible to the eye in solution.

For ZnTPPc the dimerisation free energy (taken to be the depth of the minimum at r ~ 4 Å) varies significantly with the protonation state of the molecule, with the dimerisation free energy for the H_4[ZnTPPc] - H_4[ZnTPPc] pair being approximately three times that of the other combinations (Figure S8c). The increased stability of the H_4[ZnTPPc] - H_4[ZnTPPc] pair compared to the others may be due to stronger hydrophobic interactions. The latter is in agreement with the kinetic instability of the neutral porphyrin species, experimentally observed to precipitate rapidly for pH conditions across the range of $4.0 \leq pH \leq 5.5$ (see Figure S9). Across this pH range, the steric influence of the axial water molecule alone is no longer sufficient to prevent the close approach of two H_4[ZnTPPc] species due to minimisation of electrostatic repulsion, leading to stronger hydrophobic interactions. The PMF calculations show significant structure with a number of minima spaced ~2-3 Å apart. These may arise due to water molecules interacting with the zinc centre. Such structure is much less apparent for H_2TPPc (Figure S8d), which lacks the zinc centre. For this case the dimerisation free energy is higher than for ZnTPPc and is less influenced by the protonation states of the molecules. Again, this finding fits with the experimentally observed deviation of H_2TPPc from the Beer-Lambert law due to rapid dimerisation in aqueous solutions (Figure S8b), even at pH values $\geq p\mathit{K}a^{COOH}$ where ZnTPPc remains in monomeric form.

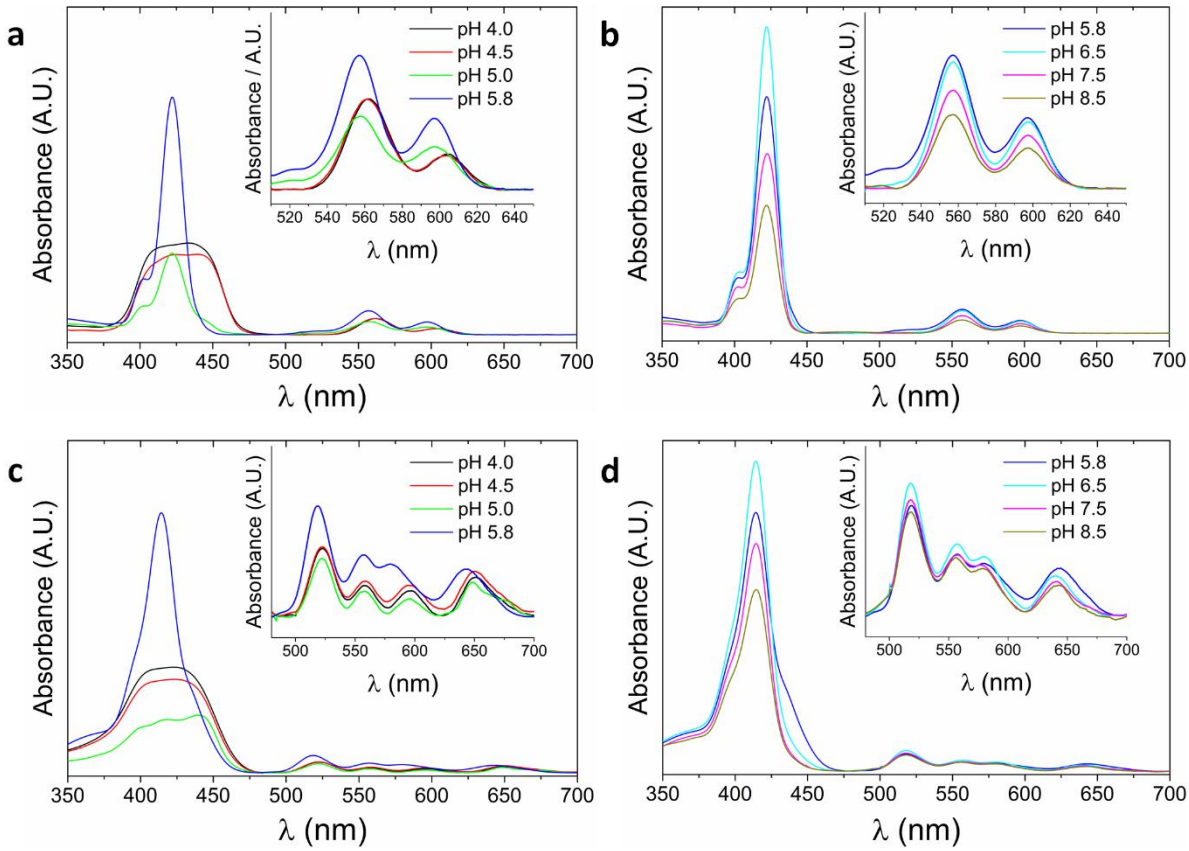

Figure S9. Investigating the tendency of the porphyrin molecules in the aqueous solution to aggregate: influence of pH. UV/vis absorbance spectra of aqueous solutions of 50 μM ZnTPPc at pH conditions a) more acidic and b) more alkaline than p*K*a^{COOH} (= pH 5.8). Identical experiments were performed with 50 μM H_2TPPc at pH conditions c) more acidic and d) more alkaline than p*K*a^{COOH}. The pH of each aqueous solution was adjusted using citric acid and LiOH. The ionic strength at each pH condition was maintained at 10 (±2) mM. Insets: The Q-band region of the ZnTPPc and H_2TPPc UV/vis absorbance spectra.

Discussion | As the pH becomes progressively more acidic than p*K*a^{COOH}, the equilibrium is displaced towards the neutral H_4[ZnTPPc] or H_4[H_2TPPc] species relative to the anionic [ZnTPPc]$^{4-}$ or [H_2TPPc]$^{4-}$ species. As noted in Figures S8c and S8d, the H_4[ZnTPPc] - H_4[ZnTPPc] pair (or H_4[H_2TPPc]- H_4[H_2TPPc] pair) is stable due to strong hydrophobic

interactions, leading to kinetic instability and rapid bulk aggregation. The latter explains the reduction in peak intensity and broadening of the Soret bands across the range of $4.0 \leq pH \leq 5.5$ for ZnTPPc and H_2TPPc in Figures S8a and S8c, respectively.

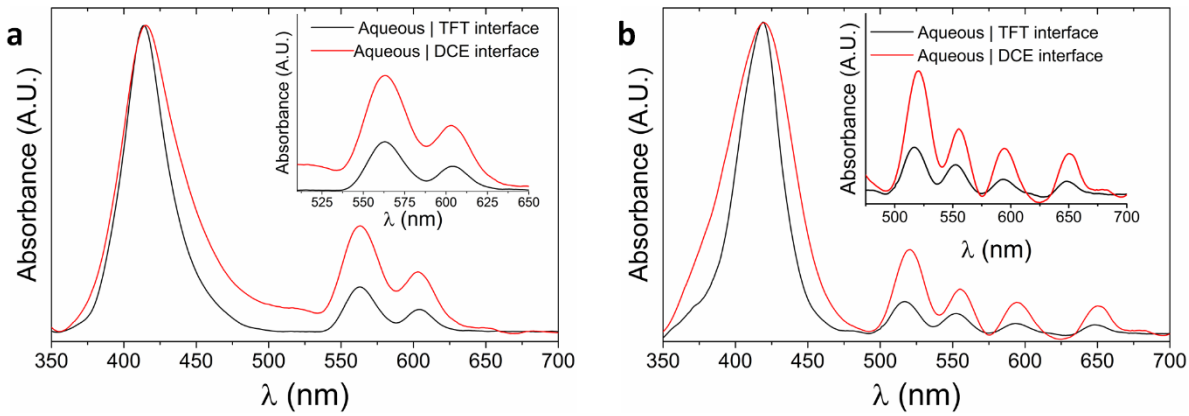

Figure S10. Investigating the formation of porphyrin interfacial aggregates at the aqueous-organic interface: influence of the organic solvent. UV/vis absorbance spectra of a) ZnPor-INs and b) H_2Por-INs self-assembled as described in Figure 1 for 24 hours with 50 μM porphyrin in the aqueous phase and either an α,α,α-trifluorotoluene (TFT) or 1,2-dichloroethane (DCE) organic phase. The UV/vis spectra with each organic solvent were normalized to the maximum absorbance of the Soret bands of the ZnPor-INs (λ_{max} = 414 nm) or H_2Por-INs (λ_{max} = 420 nm), respectively. Insets: The Q-band region of the ZnPor- and H_2Por-INs UV/vis absorbance spectra.

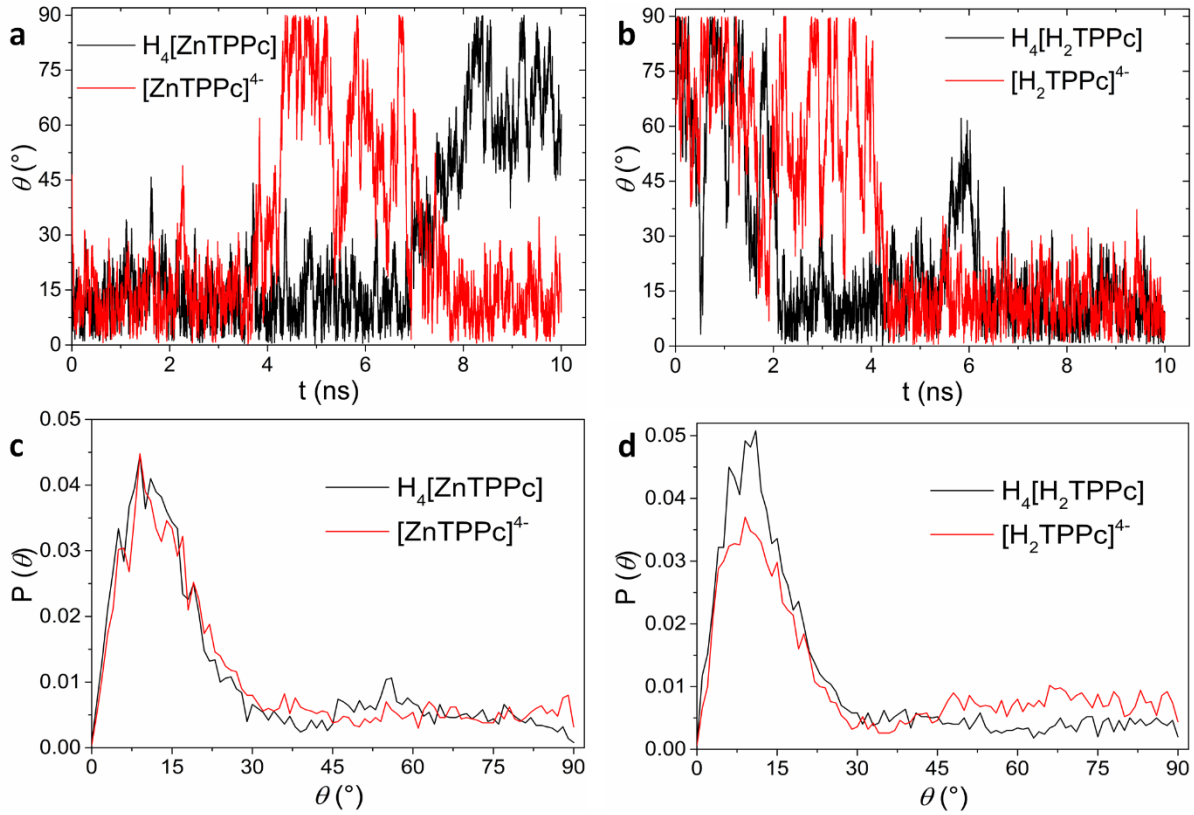

Figure S11. Simulations of the average angle of orientation, θ, of fully protonated (black lines) and fully deprotonated (red lines) **a)** ZnTPPc and **b)** H_2TPPc molecules *versus* time at the water | TFT interface. Probability distributions of the angle of orientation, P(θ), of fully protonated (black lines) and fully deprotonated (red lines) **c)** ZnTPPc and **d)** H_2TPPc molecules average over 10 ns of molecular dynamics (MD).

Discussion | Regardless of the presence of the zinc centre and protonation state, there is a significant degree of orientational freedom (Figure S11a,b), with all molecules adopting a range of orientations relative to the interface. This is reflected in the orientational angle probability distributions (Figure S11c,d) which have peaks at low (<15°) angle but remain non-zero for all angles.

Assuming perfectly flat lying molecules in a monolayer of the interdigitated clathrate structure obtained from the XRD analysis, the theoretical monolayer concentration of the ZnPor-INs (Γ_m) was calculated as 5.74 x 10^{13} molecules·cm^{-2} or 0.0948 nmol·cm^{-2} (assuming the area of a single ZnTPPc molecule as 2.25 nm^2).[20] Experimentally the value obtained from the ZnTPPc absorption isotherm is two orders of magnitude greater at 13.1 nmol·cm^{-2}. The discrepancy between the theoretical and experimental values can be attributed to the non-zero dihedral angle of the ZnTPPc molecules at the liquid | liquid interface, the presence of overlapping regions in the clathrate structure and the presence of porphyrin amorphous domains.

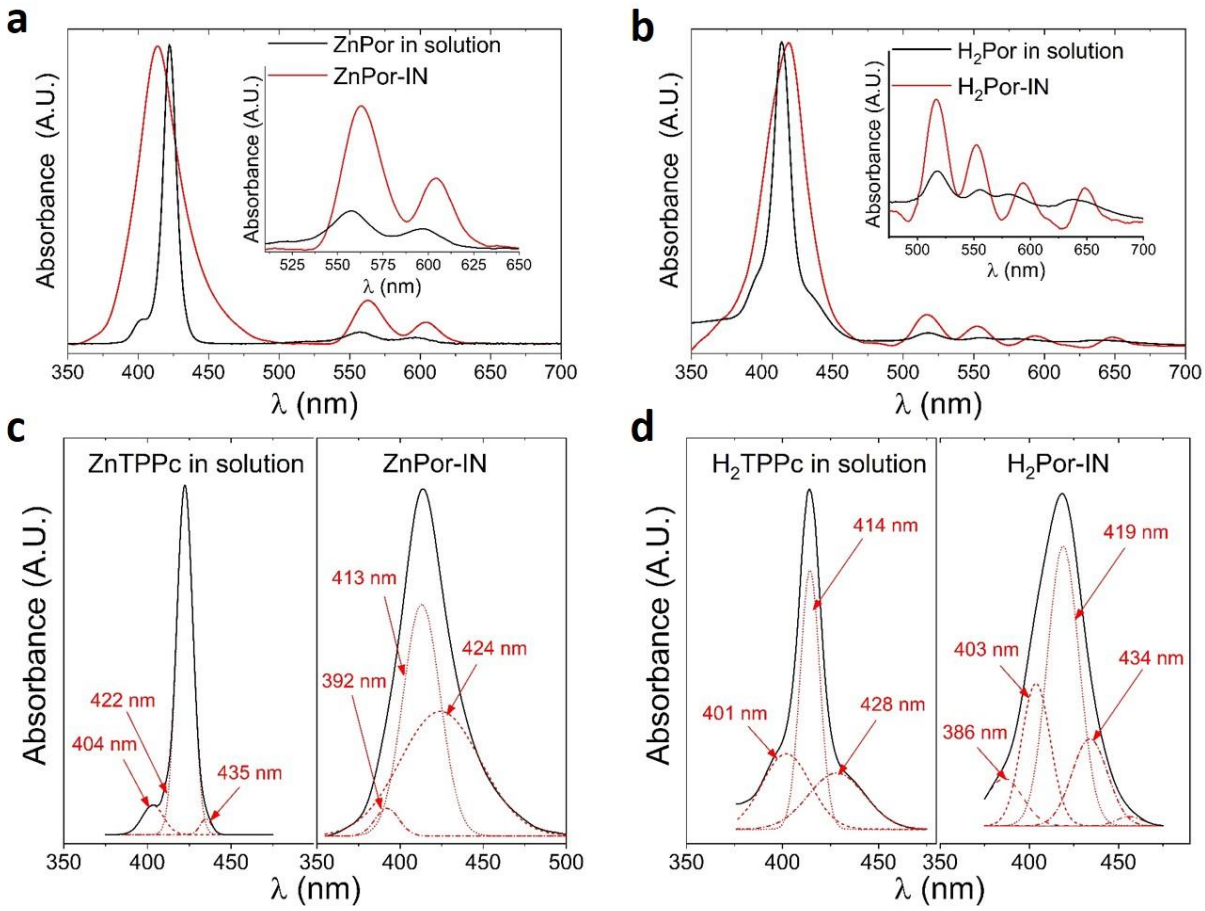

Figure S12. Comparison of the *in situ* UV/vis absorption spectra for **a,c** ZnTPPc in solution *versus* ZnPor-INs and **b,d** H_2TPPc in solution *versus* H_2Por-INs. The porphyrin aqueous solutions consisted of either 50 μM ZnTPPc or H_2TPPc in lithium citrate buffer (10 mM ionic strength, pH 5.8). The Por-INs were self-assembled as described in Figure 1 for 24 hours with either 50 μM ZnTPPc or H_2TPPc in the aqueous phase. The *in situ* UV/vis absorbance spectra of the Por-INs were normalized to the maximum absorbance of the Soret bands of ZnTPPc (λ_{max} = 422 nm) or H_2TPPc (λ_{max} = 414 nm) in solution, respectively. Insets: The Q band region of the *in situ* UV/vis absorption spectra.

Table S1. The absorption maxima ($\lambda_{max.}$) of the Soret and Q bands of both ZnTPPc and H_2TPPc in 10 mM lithium citrate buffer solution (pH 5.8), and their corresponding Por-INs self-assembled at the immiscible water|TFT interface.

Porphyrin species	*Absorption peaks (nm)*				
	Soret[a,b]	Q(1,0)		Q(0,0)	
ZnTPPc in solution	422 (11)	557		596	
ZnTPPc interfacial nanostructures	413 (35)	563		604	
	Soret	Q(1,0)*y*	Q(0,0)*y*	Q(1,0)*x*	Q(0,0)*x*
H_2TPPc in solution	414 (15)	518	555	582	639
H_2TPPc interfacial nanostructures	419 (34)	517	552	593	648

[a] Accuracy of the absorption maxima is ±1 nm. [b] Values in the brackets are the full width at half maximum (FWHM) of the Soret bands. The latter are provided to highlight the extent of spectral broadening upon porphyrin nanostructure formation.

Discussion | The $\lambda_{max.}$ values of the Soret and Q bands in solution are within ±2 nm of previously reported values for spectra of ZnTPPc[21] and H_2TPPc,[17,22–25] respectively, recorded in comparable aqueous phases.

The H_2Por-INs display four Q bands, indicating that the porphyrin ring retains the D_{2h} symmetry typical of single H_2TPPc molecules. Best fits of the H_2TPPc and H_2Por-IN Soret bands required multiple peaks, each related to different vibronic transitions, revealing the co-existence of monomers and dimers in solution for H_2TPPc and domains with slight variations in the geometric arrangements of the porphyrins within the Por-INs (Figure S12d).

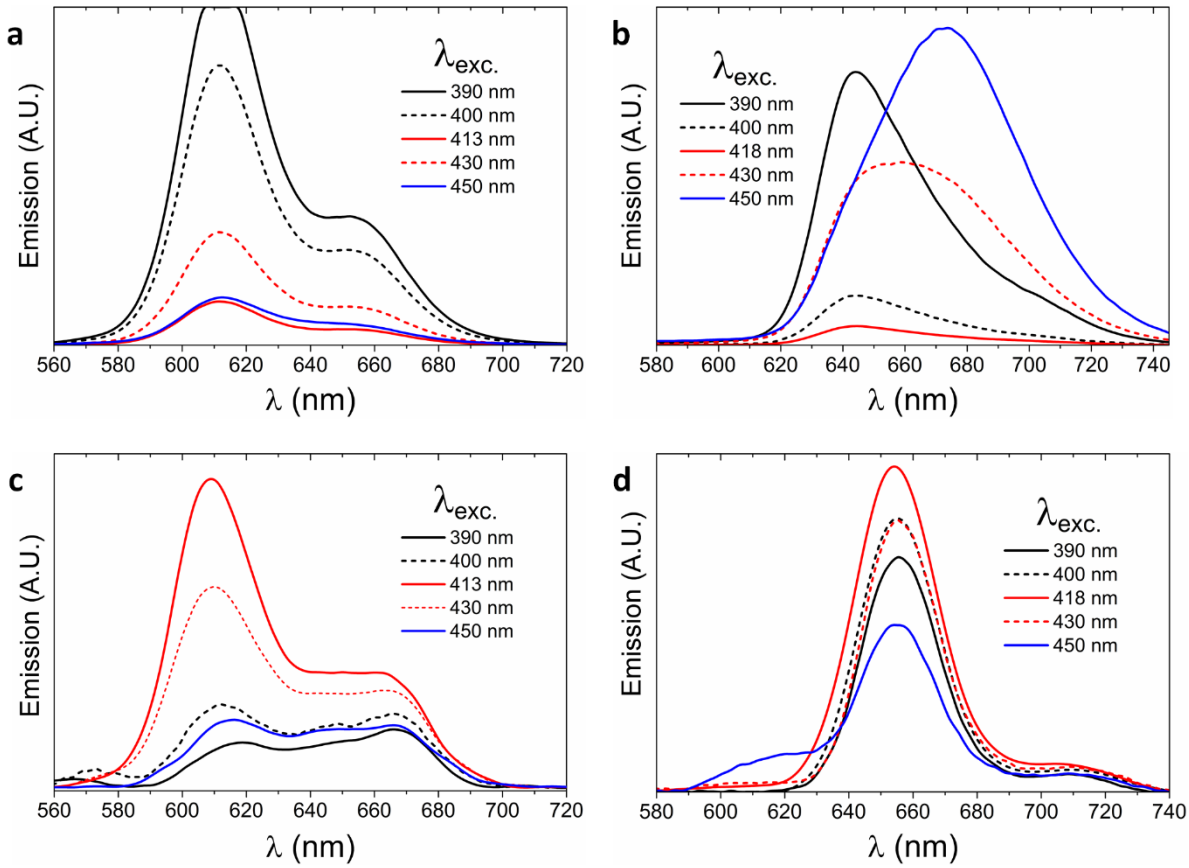

Figure S13. *In situ* steady-state fluorescence spectra as a function of excitation wavelength ($\lambda_{exc.}$) for **a**) 50 μM ZnTPPc and **b)** 50 μM H_2TPPc in 10 mM lithium citrate buffer (pH 5.8), and **c)** ZnPor-INs and **d)** H_2Por-INs self-assembled as described in Figure 1 for 24 hours with 50 μM ZnTPPc or H_2TPPc, respectively, in the aqueous phase.

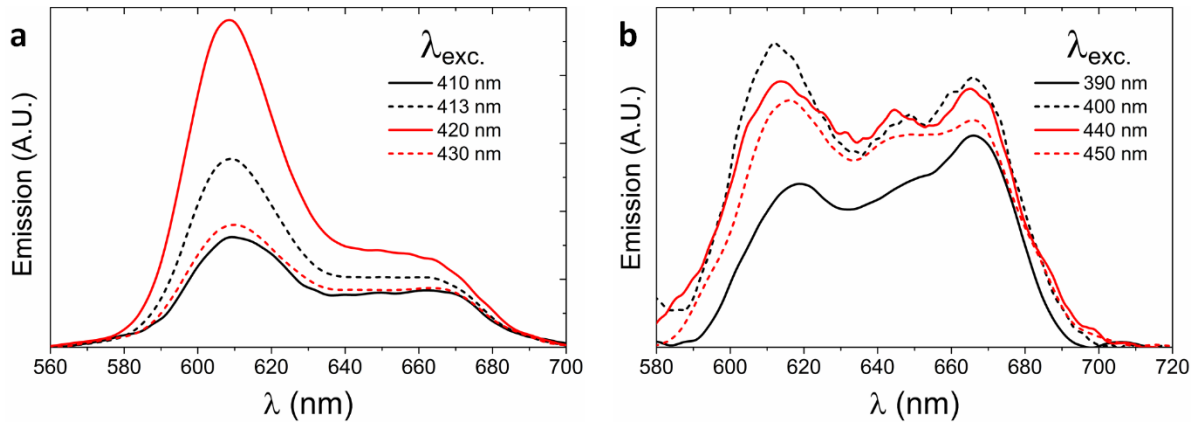

Figure S14. Two different emission regimes were observed for the *in situ* steady-state fluorescence spectra of the ZnPor-INs as a function of excitation wavelength ($\lambda_{exc.}$).

Discussion | *In situ* steady-state fluorescence spectroscopy was employed to investigate the effect of nanostructure formation on the electronic structure of the Por-INs. An assumption was made that the emission spectrum profiles of each species (*i.e.,* monomer, dimer or Por-IN) were independent of $\lambda_{exc.}$ as long as the incident radiation falls within the Soret band (Kasha's rule). Thus, if a single species of uniform electronic structure was present, only the intensity of the emissions but not the emission spectra profiles should be affected by varying $\lambda_{exc.}$ within the Soret band. However, if a number of species with varying electronic structures were present, both the emission intensities and spectral profiles should vary significantly upon changing $\lambda_{exc.}$ within the Soret band. The latter would therefore be expected from a mixture of domains with slightly different geometric arrangements of the porphyrin molecules due to their excitation at slightly different wavelengths. Quantitative comparison of emission intensities of ZnTPPc in buffer solution and the Por-INs was hampered by scattering due to the experimental configuration (Figure S1, *vide supra*).

The emission profiles of 50 μM ZnTPPc in solution were independent of $\lambda_{exc.}$ across the Soret band indicating the presence of a monomeric ZnTPPc species only in solution (Figure S13a). A dependence of the emission profile of 50 μM H_2TPPc in solution on $\lambda_{exc.}$ across the Soret band was observed due to the co-existence of the monomer and dimer species in solution (Figure S13b). The latter was expected based on previous observations from *in situ* UV/vis spectroscopy (see Figure S8b). The emission profile of the ZnPor-INs was highly dependent on $\lambda_{exc.}$ across the Soret band. Two emission regimes were tentatively assigned, each potentially corresponding to distinct domains with slightly different geometric arrangements of the porphyrin molecules (Figures 13c and S14). The emission profile of the H_2Por-INs was independent of $\lambda_{exc.}$ across the Soret band (Figure S13d), suggesting either a single nanostructure of H_2TPPc was formed at the interface, or that any different domains in the nanostructure had very similar electronic structures.

Table S2. Assignment of the bands observed in the Raman spectra of the ZnPor- and H_2Por-INs excited at 532 nm (the experimental data is presented in Figure 4e; note that the peak at 522 cm^{-1} is due to the underlying silicon substrate).

H_2Por-IN	**ZnPor-IN**	**Assignment**[a,b]
322	-	-
-	374	-
-	408	-
705	-	Phenyl
824	-	Phenyl
966	-	Phenyl
1005	1009	Phenyl, $\nu(C_\alpha\text{-}C_M)$
-	1031	Phenyl
1086	1076	A_{1g}, $\delta_s(C_\beta\text{-H})$
1140	-	A_{1g}, $\nu(C_\alpha\text{-N})$
-	1179	Phenyl
1241	1243	$\nu(C_M\text{-}\Phi)$
1327	-	B_{1g}, $\nu_{as}(C_\alpha\text{-N})$
1364	-	A_{1g}, $\nu_s(C_\alpha\text{-N}) + \nu_s(C_\alpha\text{-}C_\beta)$
-	1354	A_{1g}, $\nu_s(C_\alpha\text{-}C_\beta) + \nu_s(C_\alpha\text{-N})$
1453	1450	B_{1g}, $\nu_{as}(C_\beta\text{-}C_M)$
-	1496	B_{1g}, $\nu(C_\beta\text{-}C_\beta)$
1555	1550	A_{1g}, $\nu(C_\beta\text{-}C_\beta)$
1606	1605	Phenyl

[a] ν represents bond stretching and δ represents bond bending. Subscripts s and as refer to the symmetric and asymmetric vibrations with respect to the pyrrole 2-fold axis for $\nu(C_\beta\text{-H})$, $\delta(C_\beta\text{- H})$, $\nu(C_\alpha\text{-N})$, or the methine 2-fold axes for $\nu(C_\alpha\text{-}C_\beta)$. Φ represents the phenyl group. [b] Assignments from references [26–29].

Discussion | Firstly, the peak at 322 cm^{-1} for the H_2Por-INs is absent for the ZnPor-INs, with two peaks at 374 and 408 cm^{-1} observed instead. Secondly, the single peak at 1354 cm^{-1} for the ZnPor-INs is replaced by a doublet at 1327 and 1364 cm^{-1} for the H_2Por-INs. Furthermore, as noted by Vlčková *et al.* when comparing surface-enhanced resonance Raman spectra (SERRS) of free-base and silver H_2TPPc species,[28] a major distinguishing factor is a loss in intensity of the

phenyl out-of-plane modes and a gain in intensity of the phenyl in-plane modes upon metalation. For example, bands at 705, 824 and 966 cm^{-1}, associated with π_3, π_2 and π_1 phenyl ring out-of-plane modes (mode orders from Spiro and co-workers)[30,31] are present in the H_2Por-IN spectra, but absent in the ZnPor-IN spectra. Additionally, the phenyl ring in-plane mode at 1179 cm^{-1} present in the ZnPor-IN spectra is entirely absent in the H_2Por-IN spectra.

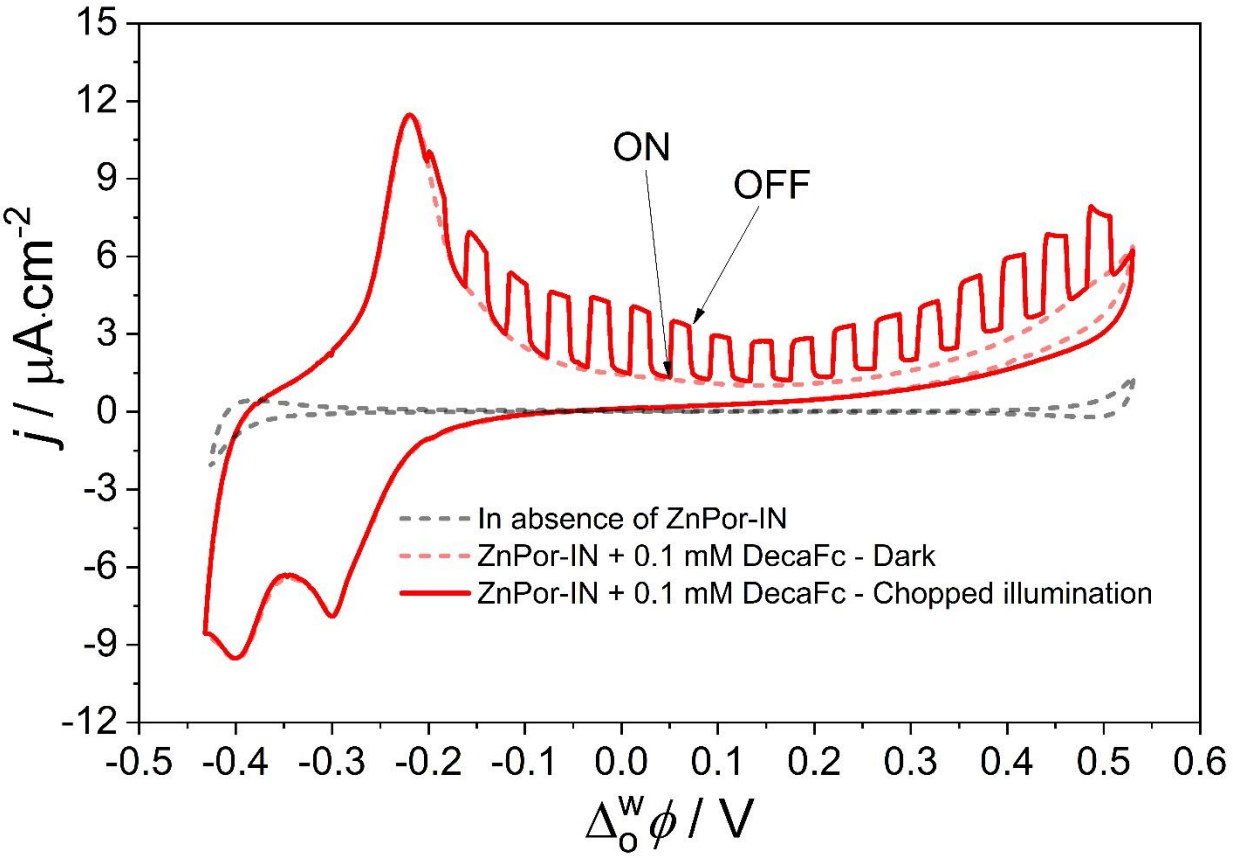

Figure S15. Photoconversion at the interface between two immiscible liquids (control cyclic voltammograms, CVs). CVs were obtained at a water|TFT interface electrified using a specialised 4-electrode electrochemical cell, as described in the Supporting Experimental Methods. The electrochemical cell configuration had 0.1 mM decamethylferrocene (DecaFc) and 5 mM bis(triphenylphosphoranylidene)ammonium tetrakis(pentafluorophenyl)borate (BATB, the supporting electrolyte) dissolved in the TFT organic phase. The aqueous phase was 10 mM ionic strength lithium citrate buffer. The ZnPor-INs floating at the water|TFT interface were prepared as described in Figure S5. CVs were obtained in the dark (solid red line) and with chopped LED illumination (dashed red line; 470 nm at 50 mW·cm^{-2}) controlled by the potentiostat. A blank CV (dashed grey line) was obtained in the dark in the absence of the ZnPor-INs.

Supporting references

(1) Wang, J. M.; Wolf, R. M.; Caldwell, J. W.; Kollman, P. A.; Case, D. A. Development and Testing of a General Amber Force Field. *J. Comput. Chem.* **2004**, *25*, 1157–1174.

(2) Peters, M. B.; Yang, Y.; Wang, B.; Füsti-Molnár, L.; Weaver, M. N.; Merz, K. M. Structural Aurvey of Zinc Containing Proteins and the Development of the Zinc AMBER Force Field (ZAFF). *J. Chem. Theory Comput.* **2010**, *6*, 2935–2947.

(3) Jakalian, A.; Jack, D. B.; Bayly, C. I. Fast, Efficient Generation of High-Quality Atomic Charges. AM1-BCC Model: II. Parameterization and Validation. *J. Comput. Chem.* **2002**, *23*, 1623–1641.

(4) Jakalian, A.; Bush, B. L.; Jack, D. B.; Bayly, C. I. Fast, Efficient Generation of High-Quality Atomic Charges. AM1-BCC Model: I. Method. *J. Comput. Chem.* **2000**, *21*, 132–146.

(5) Lin, F.; Wang, R. Systematic Derivation of AMBER Force Field Parameters Applicable to Zinc-Containing Systems. *J. Chem. Theory Comput.* **2010**, *6*, 1852–1870.

(6) Martyna, G. J.; Tobias, D. J.; Klein, M. L. Constant Pressure Molecular Dynamics Algorithms. *J. Chem. Phys.* **1994**, *101*, 4177–4189.

(7) Darden, T.; York, D.; Pedersen, L. Particle Mesh Ewald: An N·log(N) Method for Ewald Sums in Large Systems. *J. Chem. Phys.* **1993**, *98*, 10089–10092.

(8) Darve, E.; Pohorille, A. Calculating Free Energies Using Average Force. *J. Chem. Phys.* **2001**, *115*, 9169–9183.

(9) Fiorin, G.; Klein, M. L.; Hénin, J. Using Collective Variables to Drive Molecular Dynamics Simulations. *Mol. Phys.* **2013**, *111*, 3345–3362.

(10) McHale, J. L. Hierarchal Light-Harvesting Aggregates and Their Potential for Solar Energy Applications. *J. Phys. Chem. Lett.* **2012**, *3* (5), 587–597.

(11) Pasternack, R. F.; Francesconi, L.; Raff, D.; Spiro, E. Aggregation of nickel(II), copper(II), and zinc(II) Derivatives of Water-Soluble Porphyrins. *Inorg. Chem.* **1973**, *12* (11), 2606–2611.

(12) Nagatani, H.; Tanida, H.; Harada, M.; Asada, M.; Sagara, T. Polarized Total-Reflection X-Ray Absorption Fine Structure of zinc(II) Porphyrin at the Heptane−water Interface. *J. Phys. Chem. C* **2010**, *114* (43), 18583–18587.

(13) Moin, S. T.; Hofer, T. S. Zinc- and Copper-Porphyrins in Aqueous Solution – Two Similar Complexes with Strongly Contrasting Hydration. *Mol. BioSyst.* **2016**, *12* (7), 2288–2295.

(14) Nagatani, H.; Tanida, H.; Ozeki, T.; Watanabe, I. Zinc(II) Porphyrins at the Air-Water Interface as Studied by Polarized Total-Reflection X-Ray Absorption Fine Structure. *Langmuir* **2006**, *22* (1), 209–212.

(15) Tanida, H.; Nagatani, H.; Watanabe, I. Polarized Total-Reflection X-Ray Absorption Fine Structure for Self-Assembled Monolayer of Zinc Porphyrin at Air-Water Interface. *J. Chem.*

Phys. **2003**, *118* (23), 10369–10371.

(16) Moin, S. T.; Hofer, T. S. Hydration of Porphyrin and Mg–porphyrin: Ab Initio Quantum Mechanical Charge Field Molecular Dynamics Simulations. *Mol. BioSyst.* **2014**, *10* (1), 117–127.

(17) Clarke, S. E.; Wamser, C. C.; Bell, H. E. Aqueous Complexation Equilibria of Meso-tetrakis(4-Carboxyphenyl)porphyrin with Viologens: Evidence for 1:1 and 1:2 Complexes and Induced Porphyrin Dimerization. *J. Phys. Chem. A* **2002**, *106* (13), 3235–3242.

(18) Pasternack, R. F.; Huber, P. R.; Boyd, P.; Engasser, G.; Francesconi, L.; Gibbs, E.; Fasella, P.; Venturo, G. C.; Hinds, L. D. On the Aggregation of Meso-Substituted Water-Soluble Porphyrins. *J. Am. Chem. Soc.* **1972**, *94* (13), 4511–4517.

(19) Krishnamurthy, M.; Sutter, J. R.; Hambright, P. Monomer-Dimer Equilibration of Water - Soluble Porphyrins as a Function of the Co-Ordinated Metal Ion. *J. Chem. Soc. Chem. Comm.* **1975**, 13–14.

(20) Cherian, S.; Wamser, C. C. Adsorption and Photoactivity of Tetra(4-Carboxyphenyl)porphyrin (TCPP) on Nanoparticulate TiO_2. *J. Phys. Chem. B* **2000**, *104* (15), 3624–3629.

(21) Kalyanasundaram, K.; Neumannspallart, M. Photophysical and Redox Properties of Water-Soluble Porphyrins in Aqueous-Media. *J. Phys. Chem.* **1982**, *86* (26), 5163–5169.

(22) Hofstra, U.; Koehorst, R. B. M.; Schaafsma, T. J. Excited-State Properties of Water-Soluble Porphyrin Dimers. *Chem. Phys. Lett.* **1986**, *130* (6), 555–559.

(23) Maiti, N. C.; Mazumdar, S.; Periasamy, N. J- and H-Aggregates of Porphyrin−Surfactant Complexes: Time-Resolved Fluorescence and Other Spectroscopic Studies †. *J. Phys. Chem. B* **1998**, *102* (97), 1528–1538.

(24) Khairutdinov, R. F.; Serpone, N. Photoluminescence and Transient Spectroscopy of Free Base Porphyrin Aggregates. *J. Phys. Chem. B* **1999**, *103* (5), 761–769.

(25) Castriciano, M. A.; Romeo, A.; Angelini, N.; Micali, N.; Longo, A.; Mazzaglia, A.; Scolaro, L. M. Structural Features of Meso-tetrakis(4-Carboxyphenyl)porphyrin Interacting with Amino-Terminated Poly(propylene Oxide). *Macromolecules* **2006**, *39* (16), 5489–5496.

(26) Akins, D. L.; Ozcelik, S.; Zhu, H.-R.; Guo, C. Fluorescence Decay Kinetics and Structure of Aggregated Tetrakis(p-Sulfonatophenyl)porphyrin. *J. Phys. Chem.* **1996**, *100* (96), 14390–14396.

(27) Akins, D. L.; Zhu, H. R.; Guo, C. Absorption and Raman Scattering by Aggregated Meso-Tetrakis(p-Sulfonatophenyl)porphine. *J. Phys. Chem.* **1994**, *98* (14), 3612–3618.

(28) Vlčková, B.; Matějka, P.; Šimonová, J.; Čermáková, K.; Pančoška, P.; Baumruk, V. Surface-Enhanced Resonance Raman Spectra of Free Base 5,10,15,20-tetrakis(4-Carboxyphenyl)porphyrin and Its Silver Complex in Systems with Silver Colloid: Direct Adsorption in Comparison to Adsorption via Molecular Spacer. *J. Phys. Chem.* **1993**, *97*

(38), 9719–9729.

(29) Yamaguchi, H.; Nakano, M.; Itoh, K. Resonance Raman Scattering Study of the P-Cation Radicals of Magnesium, Zinc, and Copper Tetraphenylporphines. *Chemistry Lett.* **1982**, 1397–1400.

(30) Li, X. Y.; Czernuszewicz, R. S.; Kincaid, J. R.; Su, Y. O.; Spiro, T. G. Consistent Porphyrin Force Field. 1. Normal-Mode Analysis for Nickel Porphine and Nickel Tetraphenylporphine from Resonance Raman and Infrared Spectra and Isotope Shifts. *J. Phys. Chem.* **1990**, *94* (1), 31–47.

(31) Li, X. Y.; Czernuszewicz, R. S.; Spiro, T. G.; Kincaid, J. R. Consistent Porphyrin Force Field. 3. Out-of-Plane Modes in the Resonance Raman Spectra of Planar and Ruffled Nickel Octaethylporphyrin. *J. Am. Chem. Soc.* **1989**, *111* (18), 7012–7023.